Laser and microwave spectroscopy of even-parity Rydberg states of neutral ytterbium and multichannel-quantum-defect-theory analysis

H. Lehec, A. Zuliani, W. Maineult, E. Luc-Koenig, P. Pillet, and P. Cheinet*
Laboratoire Aimé Cotton, CNRS, Université Paris-Sud, ENS Cachan, Université Paris-Saclay, Bâtiment 505, 91405 Orsay, France

F. Niyaz and T. F. Gallagher†
Department of Physics, University of Virginia, Charlottesville, Virginia 22904, USA

(Received 7 May 2018; published 6 December 2018)

Measurements of high-lying even-parity $6sns\ ^1S_0$ and $6snd\ ^{1,3}D_2$ levels of neutral ^{174}Yb are presented in this paper. Spectroscopy is performed with a two-step laser excitation from the ground state $4f^{14}6s^2\ ^1S_0$, and the Rydberg levels are detected by using the field ionization method. Additional two-photon microwave spectroscopy is used to improve the relative energy accuracy where possible. The spectroscopic measurements are complemented by a multichannel-quantum-defect-theory (MQDT) analysis for the $J = 0$ and the two-coupled $J = 2$ even-parity series. We compare our results with the previous analysis of Aymar, Débarre, and Robaux [J. Phys. B: At. Mol. Phys. **13**, 1089 (1980)] and analyze the observed differences. From the MQDT models, a revised value for the first ionization limit $I_{6s} = 50443.07041(25)\ \mathrm{cm}^{-1}$ is proposed for ^{174}Yb.

DOI: 10.1103/PhysRevA.98.062506

I. INTRODUCTION

The Rydberg levels of Yb are a focus of attention for two reasons. First, two (valence) electron atoms are attractive for optical clocks based on the neutral atoms [1,2] and their ions [3,4]. The largest systematic frequency uncertainty in an optical ion clock arises from the blackbody radiation shift [5], which is determined by the ionic polarizabilities. These polarizabilities can be determined from accurate measurements of the quantum defects of the high-ℓ Rydberg levels converging to the ionic states of the clock transition [6]. For example, the polarizability of the ground $6s$ state of Yb^+ can be determined from the quantum defects of the bound $6sn\ell$ Rydberg states, where $6sn\ell$ refers to the electronic configuration of the two valence electrons: one remains in the ground $6s$ level and the Rydberg electron is in the n principal quantum number and ℓ angular momentum quantum number level. Thus the accurate energy measurement of high-ℓ Rydberg levels of Yb promises reduced uncertainties on the Yb^+ clock frequency.

The second attraction of the Rydberg states of Yb is related to cold Rydberg atom experiments. While ultracold atoms in their ground state have van der Waals interactions with a range of a few nanometers, due to their exaggerated properties ultracold Rydberg atoms have micrometer range interactions. The use of cold Rydberg atoms thus presents new possibilities in quantum physics. These include quantum simulation [7] or quantum engineering [8] with, for example, the realization of quantum gates using the dipole blockade [9–11] or the production of single photons [12]. The attraction of ytterbium is that once one electron is excited to a Rydberg state, the second valence electron, which is the single valence electron of the ionic core, is easily excited by a laser [13]. This excitation produces a doubly excited state which can decay radiatively or by autoionization. This experimental technique, called *isolated core excitation* (ICE) [14], offers several fascinating possibilities. Since the ICE autoionization spectrum depends upon the ℓ of the Rydberg electron, ICE has been used to monitor population transfer to high-ℓ $5sn\ell$ states of Sr from the optically accessible low-ℓ states [15]. The fact that ICE autoionization produces ions can also be used to image the cloud by either collecting the ion fluorescence [16] or detecting the produced ions [17]. For one-electron Rydberg atoms, other imaging [18,19] or trapping [20–22] techniques have been implemented, relying on complex schemes or compromises.

To realize the full potential of ICE as a diagnostic and manipulation technique and to determine the core polarizabilities requires a comprehensive knowledge of the spectroscopy of the atom in question. Yb has been the subject of several optical studies with pulsed lasers, in particular on even-parity levels [23–26], which have provided a wide range of spectroscopic data as well as multichannel-quantum-defect-theory (MQDT) analyses of these series, but with a typical uncertainty on the GHz scale. In addition, similar measurements [27] provide the currently accepted value for the first ionization limit of ^{174}Yb isotope $I_{6s} = 50443.08(5)\ \mathrm{cm}^{-1}$. Extensive microwave measurements connecting the Yb $6sns$, $6snp$, and $6snd$ Rydberg series have also been reported for $40 \leqslant n \leqslant 58$ [28]. While these measurements are useful for $n \geqslant 40$, they cannot be extrapolated towards lower n, where doubly excited states perturb the regularity of the bound $6sn\ell$ series.

Here we present spectroscopic measurements of high-lying even-parity $6sns\ ^1S_0$ and $6snd\ ^{1,3}D_2$ Rydberg series of Yb. We have obtained an improved accuracy of two to three orders of magnitude on the absolute level energies and extended the microwave spectroscopy to significantly lower n. These

*patrick.cheinet@u-psud.fr
†tfg@virginia.edu

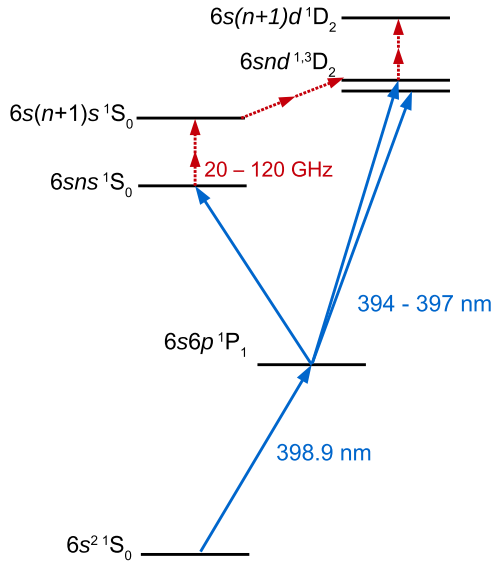

FIG. 1. Experimental energy level scheme. From the $6s^2\,{}^1S_0$ ground state, a first laser at around 398.9 nm excites atoms to the $6s6p\,{}^1P_1$ level. Then a second laser tunable around 396 nm excites the atoms to $6sns\,{}^1S_0$, $6snd\,{}^1D_2$ at UVA and also to $6snd\,{}^3D_2$ at LAC. For the singlet states, two-photon microwave transitions are performed at UVA, symbolized with red broken arrows. The blue arrows correspond to the optical spectroscopy measurements made at LAC.

levels can serve in the future as a reference for microwave spectroscopy of high-ℓ Rydberg states. In the following sections we describe the experimental approaches, present our spectroscopic results, describe the MQDT analyses of the results, and present Ritz expressions for the energies of high-lying Rydberg states.

II. EXPERIMENTAL APPROACH

We have performed joint spectroscopic measurements on two complementary setups. Both sets of measurements can be understood with the aid of Fig. 1. One cold-atom setup in Laboratoire Aimé Cotton (LAC) allows performing accurate optical spectroscopic measurements in order to obtain the absolute energies of the different observed Rydberg levels. The other experiment, at the University of Virginia (UVA), is performed on an atomic beam and allows measuring multiphoton microwave transitions between different Rydberg levels to determine their relative energy difference with better accuracy. We chose to perform our spectroscopic study on ^{174}Yb, the most abundant isotope, as the quantum defects of high-ℓ levels do not depend on the isotope. Both experiments use a two-step excitation: from $6s^2\,{}^1S_0$ to $6s6p\,{}^1P_1$ level with a first laser at 398.9 nm and a second laser at around 396 nm to reach $6sns$ and $6snd$. The UVA experiment reaches $6sns\,{}^1S_0$ and $6snd\,{}^1D_2$ levels while the LAC experiment also detects $6snd\,{}^3D_2$ levels. We now present the specific details of each experiment.

A. Microwave measurements

In the microwave experiments at UVA, atoms in a thermal beam of natural Yb pass between two horizontal plates 1.5 cm apart, where they are excited to Rydberg levels by two copropagating laser beams. These lasers are pulsed tunable dye lasers running at a 20 Hz repetition rate and excite all isotopes. This fact is not an issue as both the isotope shifts and hyperfine structure shifts between two close Rydberg levels reduce rapidly with n and no additional structure could be seen in the microwave measurements. Some broadening has been observed on a few low-n transitions, leading to a small increase in the corresponding statistical uncertainty. The laser beams cross the atomic beam at a right angle, defining the region in which the Yb Rydberg atoms interact with the microwaves. A 1 μs long microwave pulse, starting 50 ns after the laser pulses, drives one of the transitions shown by the broken arrows of Fig. 1. The microwave pulse length is chosen in order not to exceed the Rydberg state lifetime which is limited by the radiative lifetimes but also by blackbody-radiation-induced population redistribution. The microwave field is generated by an Agilent 83620A synthesized sweep generator which produces a continuous wave output from 10 MHz to 20 GHz. A General Microwave DM862D switch, which has a 10 ns transition time, is then used to produce the microwave pulses. Several frequency multipliers—a Narda DBS2640X220 active doubler, a Narda DBS4060X410 active quadrupler, a Pacific Millimeter V2WO passive doubler, and a Pacific Millimeter W3WO or D3WO passive tripler—were used to multiply the synthesizer frequency to the desired frequency. The microwaves propagate from the frequency multiplier through a WR28 waveguide feedthrough to a WR28 horn inside the vacuum chamber. Approximately 1 mW of microwave power is radiated from the horn.

Approximately 50 ns after the end of the microwave pulse a large negative voltage pulse is applied to the bottom plate to field-ionize the Rydberg atoms and eject the freed electrons from the interaction region. This delay is chosen to avoid random microwave transitions in the electric field but short enough to avoid redistribution of population by blackbody radiation. The amplitude of the field pulse is chosen to allow temporal separation of the ionization signals from the initial and final states of the microwave transition. In all cases the final state ionizes at a smaller field than the initial state, leading to an earlier field ionization signal. The freed electrons pass through a hole in the top plate and are detected by a microchannel plate (MCP) detector. The signal from the final state of the transition is recorded by a gated integrator as the microwave frequency is slowly swept across a resonance over many shots of the laser. The data are stored in a computer for later analysis. We have investigated three different two-photon microwave resonances: $6sns\,{}^1S_0 \rightarrow 6s(n+1)s\,{}^1S_0$, $6snd\,{}^1D_2 \rightarrow 6s(n+1)d\,{}^1D_2$, and $6s(n+1)s\,{}^1S_0 \rightarrow 6snd\,{}^1D_2$.

As an example of our spectra, in Fig. 2 we show the observed $6s37s \rightarrow 6s38s$ resonance which displays the typical $\mathrm{sinc}^2(f)$ Fourier transform limited behavior of the 1 μs pulsed excitation. The $6s(n+1)s$ to $6snd$ microwave transitions are the most sensitive to hyperfine splitting and isotope shifts. We thus also display as an example the $6s31s$ to $6s30d$ transition which is broadened to typically 300 kHz instead of 160 kHz. It adds a small additional uncertainty in determining the line center for ^{174}Yb of typically 30 kHz which is taken into account in the uncertainty stated in Tables I, II, and III.

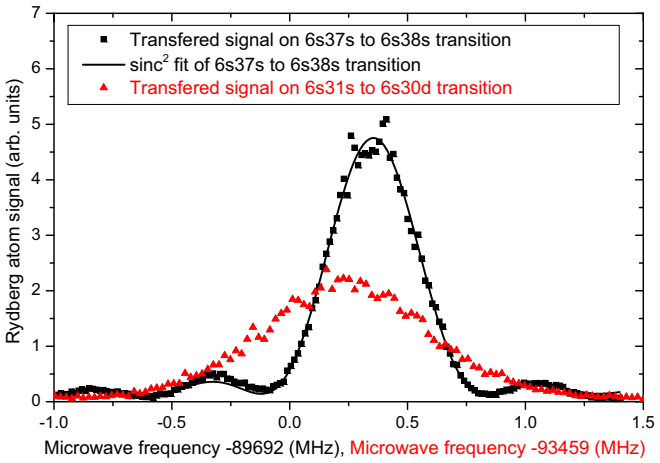

FIG. 2. Typical microwave transition line shapes. Black: Measured population in $6s38s\ ^1S_0$ level excited from $6s37s\ ^1S_0$ level as a function of the microwave excitation frequency recentered by subtracting 89692 MHz. A fit with the $\mathrm{sinc}^2(f)$ function leads to the expected Fourier transform width of 160 kHz. Red: Measured population in $6s30d\ ^1D_2$ level excited from $6s31s\ ^1S_0$ level as a function of the microwave excitation frequency recentered by subtracting 93459 MHz.

The accuracy of the two-photon microwave transitions can be limited by different error sources. The ac Stark shifts of the two-photon transitions are generally small, typically 200 kHz for the maximum power. This effect is minimized measuring the resonances at several microwave powers to extrapolate to the zero-field frequencies with an uncertainty around 20 kHz.

TABLE I. $6sns$-$6s(n+1)s$ two-photon frequencies. New measurements for $n = 34$–39 and $n = 42$ are provided with the observed statistical uncertainty. Other data are from [28]. f_{Exp} are the experimentally measured frequencies, f_{Th} are the theoretical frequencies extracted from the MQDT analysis presented later, and the last column presents their difference $f_{\mathrm{Th}} - f_{\mathrm{Exp}}$.

n	f_{Exp} (MHz)	f_{Th} (MHz)	$f_{\mathrm{Th}} - f_{\mathrm{Exp}}$ (MHz)
34	119119.66(6)	119119.73	0.07
35	108044.35(7)	108044.35	0.00
36	98299.99(6)	98299.91	−0.08
37	89692.36(6)	89692.43	0.07
38	82060.74(6)	82060.93	0.19
39	75270.32(5)	75270.92	0.60
40	69210.18	69209.62	−0.56
41	63781.70	63781.88	0.18
42	58907.08(5)	58907.03	−0.05
43	54516.42	54516.48	0.06
44	50551.50	50551.54	0.04
45	46962.06	46961.89	−0.17
46	43704.31	43704.18	−0.13
47	40740.96	40740.88	−0.08
48	38039.57	38039.53	−0.04
49	35571.81	35571.75	−0.06
50	33312.97	33312.89	−0.08
51	31241.37	31241.30	−0.07
52	29337.83	29337.94	0.11

TABLE II. $6s(n+1)s$-$6snd$ two-photon transition frequencies. New measurements for $n = 28$–39 and $n = 42$–43 are provided with the observed statistical uncertainty. Other data are from [28]. f_{Exp} are the experimentally measured frequencies, f_{Th} are the theoretical frequencies extracted from the MQDT analysis presented later, and the last column presents their difference $f_{\mathrm{Th}} - f_{\mathrm{Exp}}$.

n	f_{Exp} (MHz)	f_{Th} (MHz)	$f_{\mathrm{Th}} - f_{\mathrm{Exp}}$ (MHz)
28	117774.09(11)	117774.17	0.08
29	104637.58(11)	104637.48	−0.10
30	93459.24(6)	93459.29	0.05
31	83840.26(8)	83840.12	−0.14
32	75504.60(7)	75504.63	0.03
33	68241.11(5)	68241.25	0.14
34	61881.20(8)	61881.27	0.07
35	56288.03(9)	56287.82	−0.21
36	51348.53(7)	51348.47	−0.06
37	46970.16(5)	46970.24	0.08
38	43075.55(8)	43075.57	0.02
39	39599.77(7)	39599.57	−0.20
40	36487.09	36487.43	0.33
41	33692.83	33692.76	−0.07
42	31175.94(6)	31176.15	0.21
43	28903.64(5)	28903.86	0.22
44	26846.92	26846.97	0.05
45	24980.84	24980.57	−0.27
46	23283.35	23283.10	−0.25
47	21736.13	21735.91	−0.22
48	20322.53	20322.72	0.19

The frequency uncertainty of the synthesizer is less than 5 kHz, which leads to an uncertainty after frequency multiplication of less than 30 kHz in the worst multiplication case. The dc Stark shifts can be important on Rydberg states. For each initial state, we apply a voltage on the top plate to minimize the transition shift [29] with an estimated uncertainty of around 100 kHz. The Fourier transform limited resonance width of 160 kHz allows us to determine the resonance center with an uncertainty of around 20 kHz. The earth's magnetic field has a negligible effect on singlet-singlet transitions, as all $\Delta m = 0$ transitions are unaffected by the magnetic field [30]. Finally, the statistical noise on each measurement is around 60 kHz. We thus estimate the total uncertainty on our microwave measurements to be less than 200 kHz on the microwave frequencies and thus less than 400 kHz on the energy intervals. The uncertainty in [28] is found to be around 250 kHz on the microwave frequencies, justifying the inclusion of these data in our analysis.

B. Optical measurements

In the optical experiments at LAC, we have built an Yb cold-atom experimental setup similar to that used by Kuwamoto *et al.* [31]: a thermal beam of Yb, formed by heating a dispenser, passes through a Zeeman slower, where it is decelerated by light at the 398.9 nm $6s6p\ ^1S_0 \rightarrow 6s6p\ ^1P_1$ transition. A significant difference from the approach of Kuwamoto *et al.* is the introduction of a 2D molasses to counteract the beam divergence introduced by the Zeeman slower.

TABLE III. $6snd$-$6s(n+1)d$ two-photon transition frequencies. New measurements for $n = 32$–38 are provided with the observed statistical uncertainty. Other data are from [28]. f_{Exp} are the experimentally measured frequencies, f_{Th} are the theoretical frequencies extracted from the MQDT analysis presented later, and the last column presents their difference $f_{\mathrm{Th}} - f_{\mathrm{Exp}}$.

n	f_{Exp} (MHz)	f_{Th} (MHz)	$f_{\mathrm{Th}} - f_{\mathrm{Exp}}$ (MHz)
32	124498.32 (14)	124497.60	−0.72
33	112759.83 (6)	112759.75	−0.08
34	102451.05 (6)	102450.89	−0.16
35	93360.74 (6)	93360.56	−0.18
36	85314.28 (7)	85314.20	−0.08
37	78166.60 (7)	78166.27	−0.33
38	71794.73 (4)	71794.91	0.18
39	66097.45	66097.48	0.03
40		60987.21	
41	56390.46	56390.42	−0.04
42	52244.45	52244.19	−0.26
43	48494.83	48494.65	−0.18
44	45095.63	45095.49	−0.14
45	42006.90	42006.71	−0.19
46	39193.92	39193.70	−0.22
47	36626.62	36626.33	−0.29
48	34278.59	34278.40	−0.19
49	32127.16	32126.93	−0.23
50		30151.81	
51	28335.49	28335.32	−0.17
52	26662.12	26661.86	−0.26
53	25117.98	25117.65	−0.33
54	23690.72	23690.39	−0.33
55	22369.66	22369.27	−0.39

This 2D molasses is using 556 nm light at the $6s^2\,{}^1S_0 \rightarrow 6s6p\,{}^3P_1$ intercombination transition frequency. After the 2D molasses, the atoms are captured in a 3D magneto-optical trap (MOT) using the same intercombination transition. This trap selects a single isotope and we choose to use ^{174}Yb which is the most abundant.

To excite the atoms to Rydberg levels, the first photon is provided by the Zeeman slower laser: a fraction of continuous laser light at 398.9 nm is diverted and sent through an acousto-optical modulator (AOM) to form pulses of around 500 ns duration at a 10 Hz repetition rate. They provide population in the $6s6p\,{}^1P_1$ state. The second photon, which couples the $6s6p\,{}^1P_1$ state to the desired Rydberg state, is provided by a frequency-doubled Ti:sapphire laser. Large-n Rydberg levels are detected by pulsed field ionization. A set of high-voltage electrodes provides a maximum electric field of around 600 V/cm in the Rydberg excitation volume, allowing the ionization of Rydberg states of $n \geqslant 40$. For lower states, we use ICE with a laser at 369.5 nm on the $6s_{1/2} \rightarrow 6p_{1/2}$ ionic core transition [13] to convert bound $6sn\ell$ Rydberg atoms into autoionizing $6p_{1/2}n\ell$ atoms [32]. In all cases, the resulting ions are detected with an MCP, and the time-resolved signal is captured by a gated integrator as the frequency of the second laser is slowly swept over many shots of the laser. Figure 3 displays the obtained signal as a function of the Ti:sapphire frequency. We see a Lorentzian peak of typical

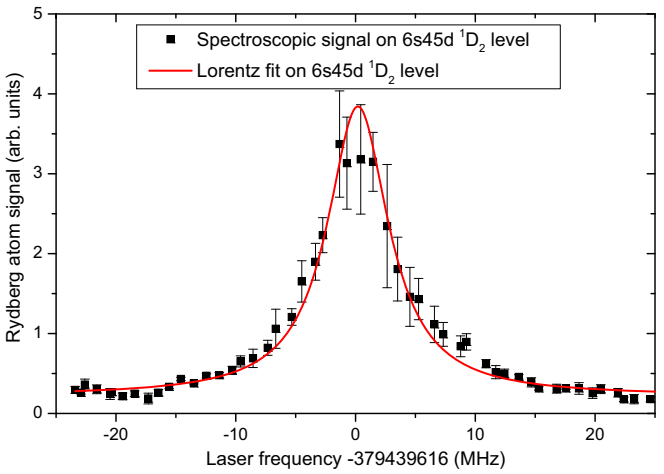

FIG. 3. Measured population in $6s45d\,{}^1D_2$ level as a function of the measured Ti:sapphire laser frequency recentered by subtracting 379439616 MHz.

width of 7 MHz from which we extract the line center rounded to 1 MHz. The width experienced by the atoms of around 14 MHz, twice the one on the Ti:sapphire, originates from a partial broadening by the intermediate state linewidth of 30 MHz.

We infer the Rydberg level energy from the sum of the $6s6p\,{}^1P_1$ intermediate level energy and the second photon energy. The energy of the intermediate level is taken to be 751 526 533.5 MHz according to the recent measurement in [33] with an uncertainty of 0.33 MHz. The corresponding laser in our experiment is servolocked to the saturated absorption signal obtained on a separate spectroscopy vacuum cell where the Yb atom beam is saturated with the intercombination laser, providing a long-term stability better than the transition linewidth of 200 kHz. The short-term stability of this laser is limited to around 2 MHz due to the width of the saturated spectroscopic signal which is broadened to the $6s6p\,{}^1P_1$ linewidth of 30 MHz. The energy of the second photon is measured using a commercial wavemeter, High Finesse WS-Ultimate 10, which we calibrate using the well known D_2 line of cesium at 852 nm available in our laboratory. The wavemeter has a guaranteed accuracy of 10 MHz at three standard deviations within ±200 nm around the calibration wavelength. To be within this range, we measure the Ti:sapphire laser frequency before the doubling stage, at around 792 nm. The uncertainty after doubling is thus 6.7 MHz at one standard deviation. The repeatability of the measurement is announced to be around 2 MHz at one standard deviation. This leads, after frequency doubling, to an expected statistical noise of 4 MHz. The dc Stark shift is minimized using compensation electrodes to cancel the residual field [29]. This field is canceled with the $6s80d\,{}^3D_2$ level, which is found to be the most sensitive. The residual uncertainty is then estimated to be at most 200 kHz. Finally the combination of the MOT magnetic field gradient, which is not turned off during the measurement, and the effect of the Zeeman slower laser pushing the MOT away from the magnetic field center leads to a residual field of around 1 G. But thanks to a linear polarization of our Rydberg excitation

laser beams, the transitions shifted up and down should have equal weight leading to a broadening but no residual shift. Therefore we assume a magnetic-field-induced uncertainty of less than 100 kHz. The total uncertainty on the Rydberg energy is thus 7.5 MHz and the statistical noise is expected to be 5 MHz.

III. RESULTS: $6sns\ ^1S_0$ SERIES

A. $6sns$ to $6s(n+1)s$ microwave transitions

We first present the data for the microwave transitions $6sns\ ^1S_0 \rightarrow 6s(n+1)s\ ^1S_0$ that have been measured at UVA with principal quantum number ranging from $n = 34$ to $n = 39$ plus $n = 42$. These data complement previous measurements [28], providing a larger set from $n = 34$ to $n = 52$. We stop at $n = 52$ because the $n = 53$ value in [28] appears to be in error. We report in Table I the combined microwave data, mentioning the observed statistical uncertainty of our measurements. For all the microwave transitions we present the observed frequencies, which are half the frequency intervals between the states. We compare the data set to the theoretical MQDT prediction computed thanks to these data and laser spectroscopy data presented later. Finally, Table I also presents the difference between the two. We then observe a standard deviation of around 0.15 MHz on the frequencies, leading thus to around 0.3 MHz uncertainty in the energy intervals, compatible with the expected accuracy. We note the two measurements at $n = 39$ and $n = 40$ which seem to deviate from the others. This could be the result of the transition between the two data sets with different average offsets, or to the effect of an unidentified weak perturber at around $n = 40$. This deviation is also compatible with our uncertainties and the data in Table II on the $6s40s$ to $6s39d$ transition do not display this deviation. It is therefore impossible to decide if it is simply experimental error or a weak perturbation.

B. $6sns$ laser spectroscopy

At LAC we have performed laser spectroscopic measurements of the energies of the $6sns\ ^1S_0$ states in order to obtain their absolute energies. We can excite levels from $n = 23$ to $n = 80$, and the results can be found in Table IV. In this energy range, no new perturbing state was identified. Nevertheless, in order to obtain an accurate fit over this broad energy range and to extract the ionization limit, we use an MQDT analysis, which is described later. To perform our MQDT analysis, we combined our laser and microwave spectroscopy data with the low-lying levels observed in [23]. A preliminary fit of data from [23] demonstrated a standard deviation on levels from $n = 7$ to $n = 22$ of around 3 GHz and an average shift relative to our results for $n > 22$ of around 3 GHz which we finally compensate by shifting the low-lying energy levels by 0.1 cm^{-1} (3 GHz). Wherever possible, it is beneficial to use the microwave results to compute the energy of one Rydberg level from the previous or the next. Doing so, the microwave errors accumulate and induce a residual random drift which is minimized if the starting level is chosen close to the center of the microwave data set. The drift is estimated to 0.6 MHz when starting from the $n = 42$ level which was found the closest to predictions of another preliminary fit of the laser spectroscopy data only. The obtained combined data used in our final MQDT model are also presented in Table IV.

IV. RESULTS: $6snd\ ^{1,3}D_2$ SERIES

A. $6s(n+1)s$ to $6snd$ microwave transitions

Once the energy levels of one Rydberg series have been accurately measured, they can serve as a reference to perform microwave measurements towards higher ℓ levels. Although the $6snd\ ^1D_2$ levels are optically accessible in both experiments, we will get a better accuracy for level energies with microwave transitions from $6s(n+1)s\ ^1S_0$. We thus first present in Table II the corresponding microwave transition frequencies measured at UVA.

The effective quantum defect difference between the two measured levels being smaller, transitions down to $n = 28$ are now accessible with our microwave frequency range. We thus present data from $n = 28$ to $n = 39$, plus $n = 42$ and $n = 43$ to complement previous measurements [28] to form a set from $n = 28$ to $n = 48$. To evaluate the measurement stability, we again add in Table II the frequencies obtained later from the MQDT fit and the resulting difference. This difference displays again a standard deviation in the measurement of around 0.15 MHz, compatible with the expected accuracy with no exception.

B. $6snd$ laser spectroscopy

At LAC, we have completed the laser spectroscopy measurements of the $6snd\ J = 2$ Rydberg series. Note that we detect the corresponding triplet state which is necessary for an MQDT analysis. The level energies from $n = 23$ to $n = 80$ have been measured, and the results are displayed in Table V. We then combine again the laser spectroscopy data, the microwave spectroscopy data, and $n < 23$ data from [23]. We find a quite large standard deviation of around 65 GHz for the $n < 23$ data. Moreover, the microwave data now connect the $6snd$ series to the known $6sns$ series. The energy of $6snd\ ^1D_2$ levels from $n = 28$ to $n = 48$ can thus be computed from the $6s(n+1)s\ ^1S_0$ energies predicted by the MQDT model, adding twice the transition frequency. As a consistency check, we note that the laser spectroscopy data in this energy range are compatible with the microwave computed data as can be seen in Table V. We therefore assume an uncertainty of 0.3 MHz on these energies, although this neglects the average uncertainty of the MQDT fit of $6sns\ ^1S_0$ itself.

C. $6snd$ to $6s(n+1)d$ microwave transitions

As another consistency check, we have measured the $6snd - 6s(n+1)d$ transitions. Within the available microwave frequency range we could only observe transitions for $n \geqslant 32$. We have performed the measurements for $32 \leqslant n \leqslant 38$ which complete the previous observations in [28] and the resulting data set is given in Table III. We also present the prediction from the MQDT model and the difference between the two.

We find only small discrepancies with typically around 200 kHz difference. We also notice the nonvanishing average difference, with the theoretical frequencies being generally

TABLE IV. Experimental and theoretical energies of the $6sns\ ^1S_0$ Rydberg series of ^{174}Yb. E_{LSp} is the new laser spectroscopy data. E_{Cb} is the chosen combination of experimental data to be analyzed with MQDT: Data followed with ▲ are taken from [23] minus the observed shift of 0.1 cm^{-1}, data followed with • are extrapolated from E_{LSp} at $n = 42$ with the microwave data presented in Table I, and data without sign are from E_{LSp}. E_{Th} is the theoretical energy obtained with our MQDT model presented in Table VI. The next column corresponds to the difference between theoretical and experimental energies expressed in MHz, and the last column is the quantum defect inferred from the MQDT model, computed assuming the ionization limit at 50443.07042 cm^{-1}.

Assignment	E_{LSp} (cm^{-1})	E_{Cb} (cm^{-1})	E_{Th} (cm^{-1})	$E_{Cb} - E_{\mathrm{Th}}$ (MHz)	Q. Defect
$6s7s\ ^1S_0$		34350.55▲	34350.549906	2	4.388654
$6s8s\ ^1S_0$		41939.78▲	41939.780040	–2	4.407614
$6p^2\ ^3P_0$		42436.84▲	42436.840006	–1	
$4f^{13}5d6s6p\ B$		46081.44▲	46081.439988	0	
$6s10s\ ^1S_0$		46893.14▲	46893.135007	149	4.440109
$6s11s\ ^1S_0$		47808.39▲	47808.426066	–1082	4.546200
$6p^2\ ^1S_0$		48344.28▲	48344.222696	1717	
$6s12s\ ^1S_0$		48723.39▲	48723.442248	–1567	4.011611
$6s13s\ ^1S_0$		49046.33▲	49046.346545	–497	4.136174
$6s14s\ ^1S_0$		49302.44▲	49302.604742	–4939	4.190760
$6s15s\ ^1S_0$		49499.14▲	49498.902231	7128	4.219180
$6s16s\ ^1S_0$		49649.95▲	49649.941036	268	4.237369
$6s17s\ ^1S_0$		49767.75▲	49767.685616	1930	4.253210
$6s18s\ ^1S_0$		49859.41▲	49859.328529	2442	4.289097
$4f^{13}5d6s6p\ A$		49897.22▲	49897.230880	–327	
$6s19s\ ^1S_0$		49940.64▲	49940.692904	–1587	4.220444
$6s20s\ ^1S_0$		50001.25▲	50001.051310	5956	4.243638
$6s21s\ ^1S_0$		50051.82▲	50051.873470	–1604	4.251391
$6s22s\ ^1S_0$		50094.61▲	50094.534923	2250	4.255941
$6s23s\ ^1S_0$	50130.625484	50130.625484	50130.625506	–0.66	4.259130
$6s24s\ ^1S_0$	50161.409314	50161.409314	50161.409264	1.50	4.261552
$6s25s\ ^1S_0$	50187.870220	50187.870220	50187.870190	0.88	4.263476
$6s26s\ ^1S_0$	50210.777667	50210.777667	50210.777658	0.27	4.265050
$6s27s\ ^1S_0$	50230.738543	50230.738543	50230.738567	–0.74	4.266364
$6s28s\ ^1S_0$	50248.236248	50248.236248	50248.236241	0.22	4.267477
$6s29s\ ^1S_0$	50263.659051	50263.659051	50263.659169	−3.56	4.268432
$6s30s\ ^1S_0$	50277.322237	50277.322237	50277.322373	−4.10	4.269260
$6s31s\ ^1S_0$	50289.483450	50289.483450	50289.483399	1.53	4.269983
$6s32s\ ^1S_0$	50300.354170	50300.354170	50300.354421	−7.51	4.270620
$6s33s\ ^1S_0$	50310.111320	50310.111320	50310.111484	−4.92	4.271184
$6s34s\ ^1S_0$	50318.901535	50318.901648•	50318.901631	0.49	4.271687
$6s35s\ ^1S_0$	50326.848499	50326.848456•	50326.848444	0.37	4.272137
$6s36s\ ^1S_0$	50334.056419	50334.056400•	50334.056387	0.39	4.272542
$6s37s\ ^1S_0$	50340.614223	50340.614269•	50340.614251	0.54	4.272907
$6s38s\ ^1S_0$	50346.597829	50346.597899•	50346.597886	0.38	4.273238
$6s39s\ ^1S_0$	50352.072416	50352.072403•	50352.072402	0.04	4.273539
$6s40s\ ^1S_0$	50357.093890	50357.093898•	50357.093937	−1.18	4.273814
$6s41s\ ^1S_0$	50361.711017	50361.711104•	50361.711106	−0.07	4.274066
$6s42s\ ^1S_0$	50365.966161	50365.966161	50365.966175	−0.42	4.274297
$6s43s\ ^1S_0$	50369.896147	50369.896018•	50369.896029	−0.34	4.274509
$6s44s\ ^1S_0$	50373.532996	50373.532962•	50373.532977	−0.45	4.274705
$6s45s\ ^1S_0$	50376.905462	50376.905396•	50376.905413	−0.51	4.274886
$6s46s\ ^1S_0$	50380.038430	50380.038367•	50380.038373	−0.19	4.275054
$6s47s\ ^1S_0$	50382.953980	50382.954005•	50382.954002	0.09	4.275209
$6s48s\ ^1S_0$	50385.671794	50385.671949•	50385.671941	0.23	4.275354
$6s49s\ ^1S_0$	50388.209683	50388.209676•	50388.209665	0.34	4.275489
$6s50s\ ^1S_0$	50390.582791	50390.582772•	50390.582757	0.45	4.275615
$6s51s\ ^1S_0$	50392.805062	50392.805174•	50392.805154	0.59	4.275732
$6s52s\ ^1S_0$	50394.889104	50394.889374•	50394.889349	0.74	4.275842
$6s53s\ ^1S_0$	50396.846524	50396.846583•	50396.846566	0.51	4.275946

TABLE IV. (*Continued.*)

Assignment	E_{LSp} (cm^{-1})	E_{Cb} (cm^{-1})	E_{Th} (cm^{-1})	$E_{Cb} - E_{\mathrm{Th}}$ (MHz)	Q. Defect
$6s54s\ ^1S_0$	50398.686864	50398.686864	50398.686912	−1.46	4.276043
$6s55s\ ^1S_0$	50400.419329	50400.419329	50400.419511	−5.45	4.276134
$6s56s\ ^1S_0$	50402.052459	50402.052459	50402.052610	−4.52	4.276219
$6s57s\ ^1S_0$	50403.593725	50403.593725	50403.593684	1.23	4.276300
$6s58s\ ^1S_0$	50405.049399	50405.049399	50405.049519	−3.60	4.276377
$6s59s\ ^1S_0$	50406.426285	50406.426285	50406.426287	−0.07	4.276449
$6s60s\ ^1S_0$	50407.729587	50407.729587	50407.729611	−0.72	4.276517
$6s61s\ ^1S_0$	50408.964441	50408.964441	50408.964623	−5.46	4.276581
$6s62s\ ^1S_0$	50410.135851	50410.135851	50410.136014	−4.90	4.276642
$6s63s\ ^1S_0$	50411.248021	50411.248021	50411.248081	−1.79	4.276700
$6s64s\ ^1S_0$	50412.304819	50412.304819	50412.304761	1.72	4.276755
$6s65s\ ^1S_0$	50413.309647	50413.309647	50413.309674	−0.81	4.276808
$6s66s\ ^1S_0$	50414.266242	50414.266242	50414.266145	2.90	4.276857
$6s67s\ ^1S_0$	50415.177206	50415.177206	50415.177239	−0.99	4.276905
$6s68s\ ^1S_0$	50416.045807	50416.045807	50416.045781	0.77	4.276950
$6s69s\ ^1S_0$	50416.874380	50416.874380	50416.874380	−0.02	4.276993
$6s70s\ ^1S_0$	50417.665460	50417.665460	50417.665449	0.33	4.277034
$6s71s\ ^1S_0$	50418.421250	50418.421250	50418.421219	0.91	4.277073
$6s72s\ ^1S_0$	50419.143750	50419.143750	50419.143761	−0.34	4.277111
$6s73s\ ^1S_0$	50419.835028	50419.835028	50419.834993	1.03	4.277146
$6s74s\ ^1S_0$	50420.496619	50420.496619	50420.496700	−2.42	4.277181
$6s75s\ ^1S_0$	50421.130458	50421.130458	50421.130538	−2.39	4.277213
$6s76s\ ^1S_0$	50421.737944	50421.737944	50421.738051	−3.20	4.277245
$6s77s\ ^1S_0$	50422.320814	50422.320814	50422.320676	4.12	4.277275
$6s78s\ ^1S_0$	50422.879734	50422.879734	50422.879756	−0.66	4.277304
$6s79s\ ^1S_0$	50423.416439	50423.416439	50423.416541	−3.05	4.277332
$6s80s\ ^1S_0$	50423.932196	50423.932196	50423.932201	−0.16	4.277358

TABLE V. Experimental and theoretical energies of the $6snd\ ^{1,3}D_2$ Rydberg series of ^{174}Yb. E_{LSp} is the new laser spectroscopy data. E_{Cb} is the chosen combination of experimental data to be analyzed with MQDT: Data followed with ▲ are taken from [23], data followed with • are extrapolated from $6s(n+1)s$ with the microwave data presented in Table II, and data without sign are from E_{LSp}. E_{Th} is the theoretical energy obtained with our MQDT model presented in Table VIII. The next column corresponds to the difference between theoretical and experimental energies expressed in MHz, and the last column is the quantum defect inferred from the MQDT model, computed assuming the ionization limit at 50443.07040 cm^{-1}.

Assignment	E_{LSp} (cm^{-1})	E_{Cb} (cm^{-1})	E_{Th} (cm^{-1})	$E_{Cb} - E_{\mathrm{Th}}$ (MHz)	Q. Defect
$6s8d\ ^1D_2$		46405.62▲	46403.220405	71940	2.788127
$6s8d\ ^3D_2$		46467.69▲	46468.006828	–9499	2.745826
$6p^2\ ^1D_2$		47420.97▲	47421.203636	–7005	
$6s9d\ ^1D_2$		47821.74▲	47822.561106	–24620	2.528818
$6s9d\ ^3D_2$		47634.40▲	47634.215002	5546	2.749543
$6s10d\ ^1D_2$		48403.49▲	48394.839809	259300	2.680405
$6s10d\ ^3D_2$		48357.63▲	48353.122376	135100	2.753826
$4f^{13}5d6s6p\ B$		48762.52▲	48764.627471	–63180	
$6s11d\ ^1D_2$		48883.12▲	48876.949819	185000	2.629259
$6s11d\ ^3D_2$		48838.14▲	48836.053145	62560	2.736459
$6s12d\ ^1D_2$		49176000▲	49177.269330	–38050	2.689055
$6s12d\ ^3D_2$		49161.12▲	49161.794071	–20210	2.745455
$6s13d\ ^1D_2$		49408.58▲	49409.033108	–13580	2.698312
$6s13d\ ^3D_2$		49399.10▲	49399.204959	–3147	2.746923
$6s14d\ ^1D_2$		49583.28▲	49583.268280	351	2.702633
$6s14d\ ^3D_2$		49576.36▲	49576.395882	–1076	2.747514
$6s15d\ ^1D_2$		49717.15▲	49717.113377	1097	2.705213
$6s15d\ ^3D_2$		49712.11▲	49712.054327	1669	2.747830
$6s16d\ ^1D_2$		49822.08▲	49822.053773	786	2.706943
$6s16d\ ^3D_2$		49818.19▲	49818.197542	–227	2.748024

TABLE V. (*Continued.*)

Assignment	E_{LSp} (cm^{-1})	E_{Cb} (cm^{-1})	E_{Th} (cm^{-1})	$E_{Cb} - E_{\mathrm{Th}}$ (MHz)	Q. Defect
$6s17d\ ^1D_2$		49905.79▲	49905.817505	–825	2.708195
$6s17d\ ^3D_2$		49902.78▲	49902.800583	–618	2.748154
$6s18d\ ^1D_2$		49973.69▲	49973.727869	–1136	2.709154
$6s18d\ ^3D_2$		49971.34▲	49971.318753	636	2.748247
$6s19d\ ^1D_2$		50029.61▲	50029.540423	2085	2.709929
$6s19d\ ^3D_2$		50027.66▲	50027.584510	2263	2.748317
$6s20d\ ^1D_2$		50076.05▲	50075.963353	2597	2.710592
$6s20d\ ^3D_2$		50074.44▲	50074.353678	2587	2.748373
$6s21d\ ^1D_2$		50115.18▲	50114.988242	5748	2.711202
$6s21d\ ^3D_2$		50113.67▲	50113.648840	634	2.748420
$6s22d\ ^1D_2$		50148.59▲	50148.105429	14530	2.711820
$6s22d\ ^3D_2$		50147.03▲	50146.981496	1454	2.748463
$6s23d\ ^1D_2$	50176.447184	50176.447184	50176.447238	−1.63	2.712546
$6s23d\ ^3D_2$	50175.499462	50175.499462	50175.499494	−0.98	2.748508
$6s24d\ ^1D_2$	50200.884090	50200.884090	50200.884131	−1.23	2.713624
$6s24d\ ^3D_2$	50200.087072	50200.087072	50200.087055	0.50	2.748567
$6s25d\ ^1D_2$	50222.082355	50222.082355	50222.082247	3.23	2.716060
$6s25d\ ^3D_2$	50221.433573	50221.433573	50221.433546	0.79	2.748695
$6s26d\ ^1D_2$	50240.290618	50240.290618	50240.290626	−0.24	2.737084
$6s26d\ ^3D_2$	50240.035775	50240.035775	50240.035785	−0.30	2.751688
$4f^{13}5d6s6p\ A$	50244.240350	50244.240350	50244.240348	0	
$6s27d\ ^1D_2$	50257.162357	50257.162357	50257.162284	2.18	2.704418
$6s27d\ ^3D_2$	50256.489825	50256.489825	50256.489877	−1.56	2.748236
$6s28d\ ^1D_2$	50271.516353	50271.516211•	50271.516216	−0.16	2.708428
$6s28d\ ^3D_2$	50270.973044	50270.973044	50270.972943	3.02	2.748380
$6s29d\ ^1D_2$	50284.302933	50284.303041•	50284.303034	0.19	2.709681
$6s29d\ ^3D_2$	50283.833875	50283.833875	50283.833968	−2.81	2.748431
$6s30d\ ^1D_2$	50295.718230	50295.718328•	50295.718332	−0.12	2.710325
$6s30d\ ^3D_2$	50295.305744	50295.305744	50295.305642	3.07	2.748460
$6s31d\ ^1D_2$	50305.947573	50305.947641•	50305.947632	0.26	2.710733
$6s31d\ ^3D_2$	50305.580853	50305.580853	50305.580969	−3.47	2.748480
$6s32d\ ^1D_2$	50315.148605	50315.148609•	50315.148611	−0.07	2.711022
$6s32d\ ^3D_2$	50314.820778	50314.820778	50314.820656	3.67	2.748494
$6s33d\ ^1D_2$	50323.454151	50323.454188•	50323.454197	−0.28	2.711242
$6s33d\ ^3D_2$	50323.159280	50323.159280	50323.159324	−1.34	2.748506
$6s34d\ ^1D_2$	50330.976689	50330.976713•	50330.976718	−0.16	2.711416
$6s34d\ ^3D_2$	50330.710371	50330.710371	50330.710422	−1.53	2.748515
$6s35d\ ^1D_2$	50337.811617	50337.811520•	50337.811506	0.42	2.711559
$6s35d\ ^3D_2$	50337.570183	50337.570183	50337.570088	2.84	2.748523
$6s36d\ ^1D_2$	50344.039792	50344.039856•	50344.039852	0.12	2.711679
$6s36d\ ^3D_2$	50343.820307	50343.820307	50343.820231	2.27	2.748530
$6s37d\ ^1D_2$	50349.731397	50349.731398•	50349.731403	−0.14	2.711782
$6s37d\ ^3D_2$	50349.530858	50349.530858	50349.530980	−3.67	2.748536
$6s38d\ ^1D_2$	50354.946004	50354.946093•	50354.946095	−0.07	2.711872
$6s38d\ ^3D_2$	50354.762544	50354.762544	50354.762662	−3.54	2.748541
$6s39d\ ^1D_2$	50359.735651	50359.735749•	50359.735736	0.40	2.711950
$6s39d\ ^3D_2$	50359.567535	50359.567535	50359.567399	4.06	2.748545
$6s40d\ ^1D_2$	50364.145301	50364.145263•	50364.145285	−0.65	2.712019
$6s40d\ ^3D_2$	50363.990461	50363.990461	50363.990415	1.39	2.748550
$6s41d\ ^1D_2$	50368.213916	50368.213919•	50368.213914	0.15	2.712081
$6s41d\ ^3D_2$	50368.071084	50368.071084	50368.071098	−0.42	2.748553
$6s42d\ ^1D_2$	50371.975785	50371.975864•	50371.975878	−0.42	2.712137
$6s42d\ ^3D_2$	50371.843894	50371.843894	50371.843886	0.24	2.748556
$6s43d\ ^1D_2$	50375.461130	50375.461220•	50375.461235	−0.45	2.712187
$6s43d\ ^3D_2$	50375.338979	50375.338979	50375.338992	−0.41	2.748559

TABLE V. (*Continued.*)

Assignment	E_{LSp} (cm^{-1})	E_{Cb} (cm^{-1})	E_{Th} (cm^{-1})	$E_{Cb} - E_{\mathrm{Th}}$ (MHz)	Q. Defect
$6s44d\ ^1D_2$	50378.696435	50378.696447•	50378.696450	−0.08	2.712233
$6s44d\ ^3D_2$	50378.583090	50378.583090	50378.583014	2.29	2.748562
$6s45d\ ^1D_2$	50381.704916	50381.704915•	50381.704897	0.54	2.712274
$6s45d\ ^3D_2$	50381.599376	50381.599376	50381.599436	−1.81	2.748565
$6s46d\ ^1D_2$	50384.507121	50384.507300•	50384.507283	0.51	2.712312
$6s46d\ ^3D_2$	50384.409120	50384.409120	50384.409063	1.69	2.748567
$6s47d\ ^1D_2$	50387.121930	50387.122020•	50387.122005	0.45	2.712347
$6s47d\ ^3D_2$	50387.030400	50387.030400	50387.030375	0.74	2.748569
$6s48d\ ^1D_2$	50389.565354	50389.565438•	50389.565451	−0.40	2.712380
$6s48d\ ^3D_2$	50389.479828	50389.479828	50389.479832	−0.12	2.748571
$6s49d\ ^1D_2$	50391.852203	50391.852203	50391.852260	−1.70	2.712409
$6s49d\ ^3D_2$	50391.772081	50391.772081	50391.772135	−1.61	2.748573
$6s50d\ ^1D_2$	50393.995485	50393.995485	50393.995538	−1.58	2.712437
$6s50d\ ^3D_2$	50393.920367	50393.920367	50393.920445	−2.33	2.748575
$6s51d\ ^1D_2$	50396.006944	50396.006944	50396.007050	−3.17	2.712463
$6s51d\ ^3D_2$	50395.936562	50395.936562	50395.936575	−0.38	2.748576
$6s52d\ ^1D_2$	50397.897318	50397.897318	50397.897379	−1.83	2.712486
$6s52d\ ^3D_2$	50397.831139	50397.831139	50397.831150	−0.32	2.748578
$6s53d\ ^1D_2$	50399.676015	50399.676015	50399.676067	−1.57	2.712509
$6s53d\ ^3D_2$	50399.613772	50399.613772	50399.613748	0.70	2.748579
$6s54d\ ^1D_2$	50401.351708	50401.351708	50401.351736	−0.84	2.712529
$6s54d\ ^3D_2$	50401.292934	50401.292934	50401.293024	−2.72	2.748580
$6s55d\ ^1D_2$	50402.932001	50402.932001	50402.932189	−5.64	2.712549
$6s55d\ ^3D_2$	50402.876696	50402.876696	50402.876811	−3.46	2.748581
$6s56d\ ^1D_2$	50404.424367	50404.424367	50404.424506	−4.17	2.712567
$6s56d\ ^3D_2$	50404.372197	50404.372197	50404.372214	−0.51	2.748583
$6s57d\ ^1D_2$	50405.835009	50405.835009	50405.835120	−3.34	2.712584
$6s57d\ ^3D_2$	50405.785642	50405.785642	50405.785688	−1.38	2.748584
$6s58d\ ^1D_2$	50407.169799	50407.169799	50407.169889	−2.71	2.712600
$6s58d\ ^3D_2$	50407.123100	50407.123100	50407.123111	−0.35	2.748585
$6s59d\ ^1D_2$	50408.434007	50408.434007	50408.434154	−4.40	2.712616
$6s59d\ ^3D_2$	50408.389843	50408.389843	50408.389843	−0.01	2.748585
$6s60d\ ^1D_2$	50409.632637	50409.632637	50409.632793	−4.69	2.712630
$6s60d\ ^3D_2$	50409.590674	50409.590674	50409.590779	−3.17	2.748586
$6s61d\ ^1D_2$	50410.770157	50410.770157	50410.770273	−3.47	2.712643
$6s61d\ ^3D_2$	50410.730329	50410.730329	50410.730399	−2.10	2.748587
$6s62d\ ^1D_2$	50411.850638	50411.850638	50411.850683	−1.34	2.712656
$6s62d\ ^3D_2$	50411.812745	50411.812745	50411.812806	−1.83	2.748588
$6s63d\ ^1D_2$	50412.877748	50412.877748	50412.877778	−0.91	2.712668
$6s63d\ ^3D_2$	50412.841590	50412.841590	50412.841767	−5.31	2.748589
$6s64d\ ^1D_2$	50413.854958	50413.854958	50413.855010	−1.56	2.712680
$6s64d\ ^3D_2$	50413.820734	50413.820734	50413.820744	−0.30	2.748589
$6s65d\ ^1D_2$	50414.785468	50414.785468	50414.785554	−2.60	2.712690
$6s65d\ ^3D_2$	50414.752979	50414.752979	50414.752922	1.70	2.748590
$6s66d\ ^1D_2$	50415.672415	50415.672415	50415.672339	2.28	2.712701
$6s66d\ ^3D_2$	50415.641260	50415.641260	50415.641238	0.66	2.748591
$6s67d\ ^1D_2$	50416.518067	50416.518067	50416.518065	0.07	2.712711
$6s67d\ ^3D_2$	50416.488379	50416.488379	50416.488400	−0.64	2.748591
$6s68d\ ^1D_2$	50417.325292	50417.325292	50417.325228	1.92	2.712720
$6s68d\ ^3D_2$	50417.296939	50417.296939	50417.296913	0.77	2.748592
$6s69d\ ^1D_2$	50418.096092	50418.096092	50418.096137	−1.37	2.712729
$6s69d\ ^3D_2$	50418.069206	50418.069206	50418.069092	3.42	2.748592
$6s70d\ ^1D_2$	50418.833001	50418.833001	50418.832933	2.04	2.712737
$6s70d\ ^3D_2$	50418.807117	50418.807117	50418.807081	1.07	2.748593
$6s71d\ ^1D_2$	50419.537689	50419.537689	50419.537598	2.74	2.712745

TABLE V. (*Continued.*)

Assignment	E_{LSp} (cm^{-1})	E_{Cb} (cm^{-1})	E_{Th} (cm^{-1})	$E_{Cb} - E_{\mathrm{Th}}$ (MHz)	Q. Defect
$6s71d\,^3D_2$	50419.512872	50419.512872	50419.512870	0.04	2.748593
$6s72d\,^1D_2$	50420.212022	50420.212022	50420.211973	1.47	2.712753
$6s72d\,^3D_2$	50420.188339	50420.188339	50420.188306	0.98	2.748594
$6s73d\,^1D_2$	50420.857736	50420.857736	50420.857770	−1.03	2.712760
$6s73d\,^3D_2$	50420.835120	50420.835120	50420.835104	0.48	2.748594
$6s74d\,^1D_2$	50421.476497	50421.476497	50421.476582	−2.54	2.712767
$6s74d\,^3D_2$	50421.455115	50421.455115	50421.454860	7.64	2.748595
$6s75d\,^1D_2$	50422.069907	50422.069907	50422.069890	0.50	2.712774
$6s75d\,^3D_2$	50422.049160	50422.049160	50422.049062	2.95	2.748595
$6s76d\,^1D_2$	50422.639235	50422.639235	50422.639078	4.70	2.712781
$6s76d\,^3D_2$	50422.619154	50422.619154	50422.619094	1.79	2.748596
$6s77d\,^1D_2$	50423.185412	50423.185412	50423.185435	–0.71	2.712787
$6s77d\,^3D_2$	50423.166266	50423.166266	50423.166251	0.45	2.748596
$6s78d\,^1D_2$	50423.710176	50423.710176	50423.710167	0.27	2.712793
$6s78d\,^3D_2$	50423.691829	50423.691829	50423.691740	2.67	2.748596
$6s79d\,^1D_2$	50424.214458	50424.214458	50424.214399	1.76	2.712798
$6s79d\,^3D_2$	50424.196846	50424.196846	50424.196690	4.67	2.748597
$6s80d\,^1D_2$	50424.699260	50424.699260	50424.699186	2.21	2.712804
$6s80d\,^3D_2$	50424.682115	50424.682115	50424.682158	−1.30	2.748597

smaller than the measured ones. This could be attributed to residual drift errors of the MQDT as well as the signature of a systematic shift in the microwave measurements, but all compatible with our uncertainties.

V. MULTICHANNEL-QUANTUM-DEFECT-THEORY ANALYSIS

A. Description of the method

To understand the principle behind the MQDT analysis of the Yb spectra it is helpful to begin by considering the single-channel quantum defect theory (QDT), which was developed by Seaton [34,35] and widely applied to alkali spectra. It had long been known that the energy of an n, ℓ, j (j being the total angular momentum of the electron) Rydberg state of an alkali atom can be represented by the empirical expression

$$E_{n\ell j} = I - \frac{R}{(n-\delta_{\ell j})^2} = I - \frac{R}{\nu_{n\ell j}^2}, \tag{1}$$

where I is the ionization limit, R is the Rydberg constant for the atom under study, $\delta_{\ell j}$ is the quantum defect of the ℓj series, which is to an excellent approximation constant, and $\nu_{n\ell j}$ is the level effective principal quantum number. The energies of an alkali atom are shifted from those of hydrogen by approximately $-2R\delta_{\ell j}/n^3$. Seaton realized that the origin of the constant quantum defect is the short-range interaction between the Rydberg electron and the inert ion core, which is in a $^1S_0$ state. An electron scattering from H^+ experiences a $-1/r$ Coulomb potential for all r, where r is the distance of the electron from the proton. When the electron incoming wave scatters from H^+ the scattered outgoing wave function undergoes a phase shift of π, resulting in a standing wave with a node at $r = 0$ for all electron energies. When scattering from a $^1S_0$ alkali ion such as Na^+, a Rydberg electron spends most of its time in a $-1/r$ Coulomb potential for $r \geqslant r_0$ where r_0 is the extension of the spherically symmetric ionic core. For $r < r_0$ the potential is deeper due to the incomplete screening of the nucleus charge by the electrons of the inner shells, which results in a phase shift different from π. The reflected wave of an ℓj electron, with energy $(E - I)$, exhibits a phase shift of $\mu_{\ell j}(E) + \pi$, with $\mu_{\ell j}(E = I) = \pi\delta_{\ell j}$ resulting in a standing wave phase shifted from the hydrogenic radial wave by $\mu_{\ell j}$. Since the kinetic energy of the Rydberg electron is large, ∼10 eV, when it undergoes the short-range scattering, the phase shift is approximately constant over an energy range of ∼1 eV around the ionization limit.

The solutions to the radial equation for an electron in a Coulomb potential are the regular and irregular Coulomb functions, f and g, respectively. In the classically allowed region they are oscillatory, like sines and cosines. The regular function f vanishes at $r = 0$, and the irregular function g diverges at $r = 0$. For hydrogen, the small-r boundary condition implies only the regular f functions are permissible. For bound states, the f functions vanish at $r = \infty$ at the energies for which the effective quantum number ν, defined by Eq. (1), is an integer, the principal quantum number n. For an alkali, the small-r boundary condition is applied at $r = r_0$. The radial wave function is phase shifted from the hydrogenic wave function by μ. The resulting wave function is a superposition of f and g functions with a ratio of g to f amplitudes given by $-\tan(\mu_{\ell j})$. Unlike hydrogen, at $r = \infty$ this wave function vanishes for nonintegral values of ν, specifically, those given by $\nu = n - \mu/\pi$. We recognize μ/π as the quantum defect of Eq. (1). While the discussion thus far has been focused on bound states, QDT is not limited to bound states. Since the phase μ is energy independent close to the ionization limit, the continuum waves above the ionization limit exhibit the same radial phase shift of μ relative to a hydrogenic wave function. A well known result of this phase shift is the Cooper minimum in photoionization [36].

For use in MQDT, a channel is defined by a state of the ionic core with energy I and total angular momentum J_c, as well as the incident electron orbital angular momentum ℓ and the specification of the intermediate quantum numbers defining the coupling scheme used to construct the total angular momentum J which complete the definition of the ionization channel. States with a discrete energy $E < I$ are bound levels belonging to a "closed channel" while scattering states with an energy $E > I$ belong to an "open channel." A channel wave function is the product of the wave functions for the ion core, the angular part of the Rydberg electron wave function, and the radial part of the Rydberg wave function described in the preceding paragraph. In two valence electron atoms such as alkaline-earth atoms, the Rydberg series $n_0 s_{1/2}\, n\ell_j$ converging toward the first ionization limit $n_0 s_{1/2}$ can be perturbed by doubly excited levels belonging to core-excited Rydberg series, converging towards excited ionization limits, resulting in irregular variations of the quantum defect of the levels labeled below $\delta(n, \ell, j)$.

One of the most useful tools for unraveling enormously complicated Rydberg spectra with multi-optical-electrons but a single Rydberg electron is the multichannel-quantum-defect theory (MQDT) first proposed by Seaton [34] and reformulated by Fano [37,38]. It enables one to describe the bound levels of a given Rydberg series and its adjacent continuum as well as the perturbation due to other series in terms of a small number of parameters. These parameters account for all short-range interactions between the Rydberg electron and the ionic core and describe the mixing between the different series which is responsible for the inelastic scattering of the Rydberg electron between the different ionization channels [39]. MQDT has been used both with *ab initio* calculations [39] and as a means of reducing the description of experimental complicated, perturbed spectra to a small number of meaningful parameters. Here we focus on the latter. While many formulations of MQDT have been developed [35,37,38] we describe here the "eigenchannel" MQDT formulation [37,38] which introduces two sets of channels defined in two different ranges of the Rydberg electron-ionic core distance and related by a unitary transformation matrix $U_{i\alpha}$.

First, the N "collision channels," labeled i, similar to the single channel introduced in QDT, describe at a large distance $r \geqslant r_0$ the Coulombic two-body interaction between the Rydberg electron with arbitrary energy and the singly charged ionic core in a definite energy level defining the channel ionization limit.

Second, the N "eigenchannels," labeled α, are suitable to describe at short-distance the three-body interactions between the doubly charged ionic core and the two electrons. A particular eigenchannel (also named close-coupling channel) α corresponds to a normal mode of the scattering of the Rydberg electron from the doubly charged ionic core. It describes a particular combination of Coulomb waves incoming in all the collision channels and gaining in each channel at $r \geqslant r_0$ by reflection on the doubly charged core, the same phase shift $\pi\mu_\alpha$, μ_α denoting the eigenquantum defect.

The coupling schemes used to describe both types of channels i and α are not necessarily the same. As shown by labels in Tables VI, VII, and VIII, for the i channels, the chosen scheme to couple the spin and orbital momentum of the ionic core and the Rydberg electron is the jj coupling scheme. For α channels, the Russell-Saunders LS coupling scheme is chosen. The $U_{i\alpha}$ matrix connecting the collision i channels to the eigen-α-channels can be expressed as a product of the analytically known LS-jj recoupling matrix $U_{i\overline{\alpha}}$ and a transformation matrix $V_{\alpha\overline{\alpha}}$. The key advantage of the eigenchannel formulation is that, by using the symmetry properties and estimations of the strengths of the electrostatic and spin-orbit interactions, it is possible to predict the channel couplings with a determining role. This results in the factorization of the $V_{\alpha\overline{\alpha}}$ matrix in terms of products of a few 2×2 rotation matrices, each depending on one angle θ. Indeed, for the bielectronic electrostatic interaction prevailing at small r values, its contributions are described by rotation matrices involving only two eigenchannels α and $\overline{\alpha}$ corresponding to identical Russell-Saunders LS terms. On the opposite spin-orbit interaction dominating at large r, it is associated with an analytical rotation matrix representing the LS-jj transformation for the ionization channels. The $U_{i\alpha}$ matrix is then represented by a small number of rotation angles $\theta_{\alpha\overline{\alpha}}$ resulting in a large reduction of the number of significant parameters needed in an MQDT model (for more details see Ref. [23]).

The problem is now fully parametrized with a small set of energy-independant short-range MQDT parameters (μ_α and $\theta_{\alpha\overline{\alpha}}$). The principal aim of the MQDT analysis is to determine, using the experimental energies of bound levels with the same parity Π and total angular momentum J, the optimum set of parameters (μ_α and $\theta_{\alpha\overline{\alpha}}$) predicting level energies as close as possible to all experimental data points. Following [40], we define an error function χ^2 [41] which sums all the energy differences between experimental results and model energies, normalized both with the assumed accuracy for each data and by the total number of data points such that a converged fit should lead to $\chi^2 \leqslant 1$.

The eigenchannel formulation of MQDT and its application to the calculation of observables and technical details useful in MQDT codes have been described in detail in many papers [37–39,42–46]; therefore we do not present the mathematical framework. For convenience, to lighten the discussion which follows, we summarize the working equations of MQDT used to determine the energy of the bound Rydberg levels using the notation of Ref. [43].

We consider a multichannel system composed of N channels associated with M ionization limits, so $M \leqslant N$. For any total energy E below the lowest ionization limit, labeled I_1, there are as many effective principal quantum number ν_i as there are ionization limits I_i in the model. They are defined by an equation similar to Eq. (1):

$$E = I_i - \frac{R}{\nu_i(E)^2} \tag{2}$$

for all i, from 1 to M.

At the energy E, the wave function solution of the many-channel Schrödinger equation is written at $r > r_0$ as a superposition of the wave functions in the different ionization channels i, involving in each channel the regular and irregular Coulomb functions specific to the channel and depending on ν_i and ℓ_i. In the eigenchannel representation, the coefficients of the superposition are expressed in terms of the MQDT parameters μ_α and $U_{i\alpha}$. An energy $E < I_1$ corresponds to the

energy of a bound level, when in all N channels the wave function vanishes at $r \to \infty$. A nontrivial solution exists for E satisfying the following equation:

$$\det|U_{i\alpha} \sin[\pi(\nu_i(E) + \mu_\alpha)]| = 0. \quad (3)$$

Since the values of μ_α and $U_{i\alpha}$ are fixed, Eq. (3) defines a surface in an M-dimensional ν_i space. Due to its sinusoidal dependence on ν_i it is periodic in all ν_i, and only an M-dimensional cube of linear dimension unity needs to be considered. Equation (2), which relates the different ν_i defines a line in the same M-dimensional space, and the intersection between the surface of Eq. (3) and the line of Eq. (2) determines the level energies below I_1 corresponding to the chosen values of μ_α and $U_{i\alpha}$.

A graphical way to display the perturbations of the bound Rydberg spectra by doubly excited states converging to higher-lying limits is a Lu-Fano plot [42], a plot of $-\nu_1$ vs ν_j for $I_j > I_1$. To construct a Lu-Fano plot for a multilimit system such as Yb, we must reduce the multidimensional surface defined by Eq. (3) to a line, or function $\mathcal{S}(\nu_j)$ in the Lu-Fano $(\nu_j, -\nu_1)$ plane. To this end we use Eqs. (2) to express all ν_i as a function of ν_j, except for i corresponding to the first ionization limit. The result is the function $\mathcal{S}(\nu_j)$. When there are two channels associated with I_1, the function $\mathcal{S}(\nu_j)$ is double valued.

In the $(\nu_j, -\nu_1)$ plane, Eq. (2) leads to the line $\mathcal{L}(\nu_j) = -\nu_1(\nu_j)$. Since $\nu_j \ll \nu_1$, ν_1 changes much more rapidly than ν_j and when $-\nu_1(\mathrm{mod}\ 1)$ is plotted vs $\nu_j(\mathrm{mod}\ 1)$ the result is a set of nearly vertical lines. The intersection of $\mathcal{L}$ and $\mathcal{S}$ define graphically the predicted energies. Traditionally, one plots only $\mathcal{S}$ together with the experimental $(\nu_j, -\nu_1)$ points in order to compare them with theory.

B. Application to Yb

We investigate here the ytterbium atom and more specifically the isotope ^{174}Yb. Its nuclear spin is $I = 0$ such that it displays no hyperfine structure. Its specific Rydberg constant is $R_{\mathrm{Yb}} = R_\infty * \frac{m_{\mathrm{Yb}}}{m_{\mathrm{Yb}}+m_e}$, with $R_\infty = 10973731.5685\ \mathrm{m}^{-1}$ the Rydberg constant, m_{Yb} the mass of the considered isotope, and m_e the mass of an electron. For ytterbium 174, $m_{\mathrm{Yb}} = 173.93886$ uma and we find $R = 10973696.959\ \mathrm{m}^{-1}$.

The most important assumptions in developing a relevant MQDT model to describe a discrete Rydberg spectrum, characterized in the absence of hyperfine structure by the total angular momentum J and by parity, is the choice of interacting channels contributing to the spectrum and the assumptions leading to the determinant channel couplings. Let us emphasize that a semiempirical MQDT analysis previously requires reliable information on the interacting channels and the identification of perturbers.

Our goal is to compare our present high-resolution data with a previous MQDT analysis of the Rydberg series of neutral ytterbium [23]. The general description of the MQDT models is discussed in detail in this reference which benefited from the interpretation by Wyart and Camus [24] of the energy levels of many configurations of Yb taking into account configuration mixing effects. Therefore, unless specified otherwise, we used the MQDT models introduced and described in detail in [23]. In particular for even spectra, they add a linear energy dependence of the eigenquantum defect of the Rydberg series defined by μ_α^1. The $U_{i\bar{\alpha}}$ matrix for the $6sns\ ^1S_0$ MQDT analysis is

$$U_{i\bar{\alpha}} = \begin{Bmatrix} 1 & 0 & 0 & 0 & 0 \\ 0 & 1 & 0 & 0 & 0 \\ 0 & 0 & -\sqrt{2/3} & 0 & \sqrt{1/3} \\ 0 & 0 & 0 & 1 & 0 \\ 0 & 0 & \sqrt{1/3} & 0 & \sqrt{2/3} \end{Bmatrix},$$

and the one for the $6snd\ ^{1,3}D_2$ MQDT analysis is

$$U_{i\bar{\alpha}} = \begin{Bmatrix} \sqrt{3/5} & \sqrt{2/5} & 0 & 0 & 0 \\ -\sqrt{2/5} & \sqrt{3/5} & 0 & 0 & 0 \\ 0 & 0 & 1 & 0 & 0 \\ 0 & 0 & 0 & 1 & 0 \\ 0 & 0 & 0 & 0 & 1 \end{Bmatrix}.$$

To clarify the presentation of the results, we describe briefly the ionization and close-coupling channels specific to the Yb spectrum. In this spectrum, with ground level [Xe] $4f^{14}\ 6s^2\ ^1S_0$, there exist in the presently investigated energy domain below the first ionization limit, even parity, and $J = 0$ and $J = 2$, levels belonging to configurations with two valence electrons $4f^{14}\ 6sn\ell$ and $4f^{14}\ 6p^2$ entirely located below the first ionization limit. There is also the $4f^{13}\ 5d6s6p$ configuration spread on both sides of the first limit. As in Ref. [23], we consider each perturbing level to be the lowest member of a new Rydberg series such that the channel eigenquantum defect μ_α is redundant with the ionization limit which is thus kept constant. We consider a single ionization limit for all these perturber channels, so the only free-parameter ionization limit is the first ionization limit.

C. $6sns$ MQDT analysis

We first tried the MQDT model from [23] which is based on a 5-channel model associated with the following four perturbing levels: the $6p^2\ ^3P_0$ (42436.94 cm^{-1}), the $4f^{13}5d6s6p\ B$ (46081.54 cm^{-1}), the $6p^2\ ^1S_0$ (48344.38 cm^{-1}), and the $4f^{13}5d6s6p\ A$ (49897.32 cm^{-1}). However, we have found inconsistencies with previous results using this model. The recently found optimum parameters could not reproduce the previous fit quality for $n < 23$, showed a clear residual differential drift for $n > 22$ levels, and had a minimum χ^2 of around 60 while considering an uncertainty of 3 MHz on all new data. We have thus looked for possible improvement of the model. Within the $4f^{13}5d6s6p$ configuration, the four $4f^{13}(^2F_{7/2})5d6s6p$, $J = 0$ levels are the lowest in energy and might perturb the Rydberg series. One of these levels should have a $^1S_0$ character while the three others should be $^3P_0$, two of which were already included as A and B in the original model. Another has been observed with two-photon spectroscopy from the ground state [25] at the energy of 51842.42 cm^{-1} and predicted to contain substantial $^1S_0$ character [24]. We thus suspect the influence of a perturber above the first ionization limit. Due to the absence of data on the fourth expected level, we do not know which one might explain the observed drift. We thus consider two possible options for a 6-channel model with either a direct coupling to the $6sns\ ^1S_0$ Rydberg series or a coupling to the $6pnp\ ^3P_0$ channel. In either case we add the sixth channel labeled **c**

TABLE VI. First six-channel model MQDT parameters for the $6sns\ ^1S_0$ series of ytterbium.

$i, \bar{\alpha}, \alpha$	1	2	3	4	5	6
$\|i\rangle$	$6s_{1/2}ns_{1/2}$	$4f^{13}5d6snp$ **a**	$6p_{3/2}np_{3/2}$	$4f^{13}5d6snp$ **b**	$6p_{1/2}np_{1/2}$	$4f^{13}5d6snp$ **c**
I_i	50443.070417	83967.7	80835.39	83967.7	77504.98	83967.7
$\|\bar{\alpha}\rangle$	$6sns\ ^1S_0$	$4f^{13}5d6snp$ **a**	$6pnp\ ^1S_0$	$4f^{13}5d6snp$ **b**	$6pnp\ ^3P_0$	$4f^{13}5d6snp$ **c**
μ_α^0	0.3551533	0.2045376	0.1163786	0.2954456	0.2576527	0.1560523
μ_α^1	0.2772279	0.0	0.0	0.0	0.0	0.0
$V_{\bar{\alpha}\alpha}$	$\theta_{12} = 0.1265847$	$\theta_{13} = 0.3001512$	$\theta_{14} = 0.05671288$	$\theta_{34} = 0.1142027$	$\theta_{35} = 0.09858364$	$\theta_{16} = 0.1419855$
$U_{i\alpha}$	0.9366039	−0.1262469	−0.296065	−0.01994239	0.02928208	−0.1338851
	0.119197	0.9919989	−0.03767875	−0.002537971	0.003726589	−0.01703891
	−0.2385956	0	−0.7127722	0.1024783	0.6506634	0.03410663
	0.05611209	0	0.113219	0.9918887	−0.01119784	−0.008021079
	0.1687126	0	0.6245504	−0.0724631	0.7587097	−0.02411703
	0.1415089	0	0	0	0	0.989937

(corresponding to the additional perturbing level C). We also have to extend $U_{i\bar{\alpha}}$.

We manage to find a good agreement over the whole data set with both models, obtaining a χ^2 value of around 0.81 with uncertainties set to 3 GHz for $n < 23$, 3 MHz for laser spectroscopy, and 0.6 MHz for microwave spectroscopy data. The resulting model optimum parameters are presented in Tables VI and VII. In the indirect-coupling model, the rotation angle θ_{56} is as expected much higher than the rotation angle θ_{16} of the direct-coupling model. We compare the optimum sets of our 6-channel model parameters to the set of the previous 5-channel model (Table 1 of Ref. [23]): The addition of channel **c** reduces the mixing between the Rydberg channel and the $4f^{13}5d6s6p$ **b** channel with a prevailing $^3P_0$ character [24]. Simultaneously there is a redistribution in the mixing between the $6pnp\ ^1S_0$ channel and both $4f^{13}5d6s6p$ **b** and $6pnp\ ^3P_0$ channels, the first one increasing significantly and the second one decreasing. A change in channel mixing also appears in a larger energy variation μ_α^1 in the eigenchannel quantum defect of the Rydberg series. Since level C is above the first ionization limit, it is autoionizing and its energy cannot be determined with Eq. (3) which only applies to bound levels lying below the first limit. It has been shown [35,43,47] that one can deduce the energy and the width of an autoionization resonance restricting calculations on closed channels. The first model finds an energy of 51591 cm^{-1} and a total width of 97 cm^{-1} similar to the second model which finds an energy of 51537 cm^{-1} and a total width of 89 cm^{-1}. We thus find in both models a width significantly larger than the width $\Gamma = 5$ cm^{-1} of the level observed in [25]. Two possible explanations are either that an additional perturber with large coupling is indeed present but that its width also induced a reduction in sensitivity preventing its observation, or that one needs to take into account several additional perturbers. In both cases, additional data above the first ionization limit will be necessary to verify the model.

The two models predict similar energies, with differences well below our uncertainties, and we choose to display the predicted level energies of the first model in Table IV. In the next column, we can see that the residual difference between experimental measurements and the theoretical predictions are compatible with the expected uncertainty for each point of the data set, except for $n = 40$ as discussed in the mi-

TABLE VII. Second six-channel model MQDT parameters for the $6sns\ ^1S_0$ series of ytterbium.

$i, \bar{\alpha}, \alpha$	1	2	3	4	5	6
$\|i\rangle$	$6s_{1/2}ns_{1/2}$	$4f^{13}5d6snp$ **a**	$6p_{3/2}np_{3/2}$	$4f^{13}5d6snp$ **b**	$6p_{1/2}np_{1/2}$	$4f^{13}5d6snp$ **c**
I_i	50443.070425	83967.7	80835.39	83967.7	77504.98	83967.7
$\|\bar{\alpha}\rangle$	$6sns\ ^1S_0$	$4f^{13}5d6snp$ **a**	$6pnp\ ^1S_0$	$4f^{13}5d6snp$ **b**	$6pnp\ ^3P_0$	$4f^{13}5d6snp$ **c**
μ_α^0	0.3546985	0.2045358	0.1091799	0.2967248	0.3140328	0.08932482
μ_α^1	0.2715197	0.0	0.0	0.0	0.0	0.0
$V_{\bar{\alpha}\alpha}$	$\theta_{12} = 0.126671$	$\theta_{13} = 0.3189996$	$\theta_{14} = 0.01177203$	$\theta_{34} = 0.07887204$	$\theta_{35} = -0.009607895$	$\theta_{56} = 0.9083208$
$U_{i\alpha}$	0.9418765	−0.1263325	−0.3109963	0.01345814	−0.0018379	0.002356042
	0.1199507	0.9919879	−0.03960628	0.001713933	−0.0002340618	0.0003000488
	−0.2560493	0	−0.7781676	0.06409142	0.3505288	−0.4493503
	0.01177176	0	0.07878119	0.9968221	0.0004655745	−0.0005968297
	0.1810542	0	0.5384806	−0.04531948	0.5054085	−0.6478938
	0	0	0	0	0.788472	0.6150707

TABLE VIII. The five-channel MQDT parameters for the $6snd\,^{1,3}D_2$ series of ytterbium.

$i, \bar{\alpha}, \alpha$	1	2	3	4	5
$\|i\rangle$	$6s_{1/2}nd_{5/2}$	$6s_{1/2}nd_{3/2}$	$4f^{13}5d6snp$ **a**	$4f^{13}5d6snp$ **b**	$6p_{1/2}np_{1/2}$
I_i	50443.0704	50443.0704	83967.7	83967.7	79725.35
$\|\bar{\alpha}\rangle$	$6snd\,^1D_2$	$6snd\,^3D_2$	$4f^{13}5d6snp$ **a**	$4f^{13}5d6snp$ **b**	$6pnp\,^1D_2$
μ_α^0	0.7295231	0.7522912	0.1961204	0.2336927	0.1528761
μ_α^1	−0.02289746	0.09094972	0.0	0.0	0.0
$V_{\bar{\alpha}\alpha}$	$\theta_{13} = 0.005224693$	$\theta_{14} = 0.03972731$	$\theta_{24} = -0.007083118$	$\theta_{15} = 0.1049613$	$\theta_{25} = 0.07219257$
$U_{i\alpha}$	0.7697155	0.6251608	−0.004047011	−0.02628364	−0.1265106
	−0.62847	0.7771578	0.003304371	0.03060469	0.01017855
	0.005191816	−3.798545e−005	0.9999864	−0.0002075022	−0.000545631
	0.03949828	−0.007359173	0	0.9991859	−0.003639746
	0.1047687	0.07173292	0	0	0.9919062

crowave section. The results are also displayed in a Lu-Fano representation in Fig. 4(a). Note that we added the computed $n = 9$ level as a guide to the eye. The observation of this level could improve the model in this energy range. Figure 4(b) focuses closer to the energy range of the new spectroscopic data to emphasize the accuracy improvement for $n > 22$. As previously mentioned, a slow variation of the quantum defect is observed, mainly due to the wide energy range influence of the strong perturber $6p^2\,^1S_0$ but also from at least one perturbing level above the first ionization limit.

From this fit, we extract the value for the first ionization limit of 50443.07042 cm^{-1} or 1512.2452070 THz. Once the ionization limit is extracted, we can also extract the quantum defects for each level. As the quantum defect refers to a difference in energy, it is not sensitive to the absolute uncertainty of our measurement of 7.5 MHz but only to the observed reproducibility of 3 MHz. Moreover, the quantum defects displayed in Table IV are the ones predicted by the MQDT model which averages the measurement statistical noise. Evaluating the residual uncertainty on these quantum defects is too complex, but it should at most correspond to an energy uncertainty of 3 MHz and probably below 1 MHz in the microwave data set range.

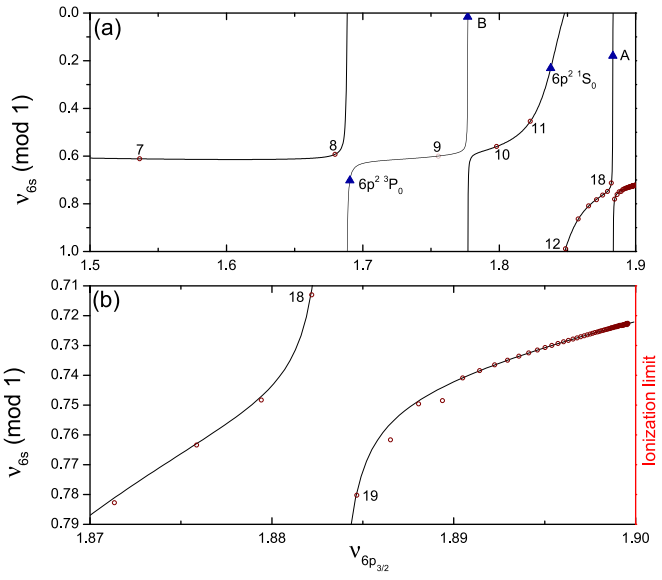

FIG. 4. Lu-Fano plot for the $6sns\,^1S_0$ series. The open circles represent the experimental positions of the $6sns$ bound states, the triangles those of the perturbers. $\nu_{6p_{3/2}}$ is calculated relative to $I_{6p_{3/2}}$ corresponding to the third channel. (a) Evolution of ν_{6s} as a function of $\nu_{6p_{3/2}}$ for the whole energy range. We add the $n = 9$ computed energy as a guide to the eye. (b) ν_{6s} evolution above the $6s15s\,^1S_0$ level.

D. $6snd$ MQDT analysis

For this Rydberg series, the 5-channel MQDT model from [23] leads to good agreement, with the expected uncertainties. It involves the three perturbing levels: $6p^2\,^1D_2$ (47420.97

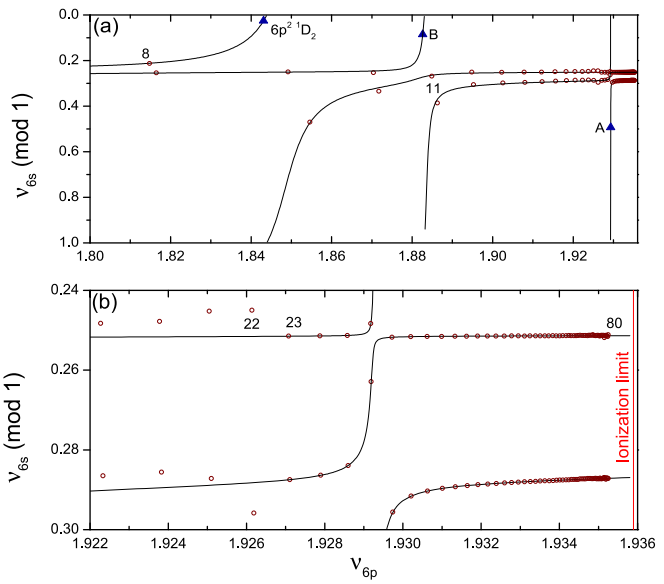

FIG. 5. Lu-Fano plot for the $6snd\,^{1,3}D_2$ series. The open circles represent the experimental positions of the $6snd$ bound states, the triangles those of the perturbers. ν_{6p} is calculated relative to I_{6p} corresponding to the fifth channel. (a) ν_{6s} evolution for the whole energy range. (b) ν_{6s} evolution above the $6s19d$ levels.

TABLE IX. Fitted Ritz parameters and validity range compatible with our experimental uncertainty. The fit is performed using the found average first ionization limit of 50443.07041 cm^{-1}. For each series we first fit the largest possible data range with coefficients up to δ_5 and perform next a fit on a restricted data range in order to maintain the accuracy with only 3 parameters.

Series	Validity range	δ_0	δ_1	δ_2	δ_3	δ_4	δ_5
$6sns\ ^1S_0$	$23 \leqslant n \leqslant 80$	4.278337	−5.625	91.65	–156050	–4.973e+7	1.102e+10
$6sns\ ^1S_0$	$34 \leqslant n \leqslant 80$	4.278312	−5.4898	−320.02			
$6snd\ ^1D_2$	$31 \leqslant n \leqslant 80$	2.713094	−1.8646	−2145.5	3940500	–3.1036e+9	1.0690e+12
$6snd\ ^1D_2$	$40 \leqslant n \leqslant 80$	2.713011	−1.1047	−373.87			
$6snd\ ^3D_2$	$28 \leqslant n \leqslant 80$	2.748679	−0.5200	−1186.01	1564600	–9.8134e+8	2.426e+11
$6snd\ ^3D_2$	$35 \leqslant n \leqslant 80$	2.748627	−0.1034	−2.10			

cm^{-1}), $4f^{13}5d6s6p\ B$ (48762.52 cm^{-1}), and $4f^{13}5d6s6p\ A$ (50244.38 cm^{-1}).

The optimum set of our 5-channel model (Table VIII) can be compared to the set of the same 5-channel model reported in Table 4 of Ref. [23]. The two sets are very similar, except for the energy variation of the eigenquantum defect in the $6snd\ ^3D_2$ series, which is strongly reduced in our description. This is due to the introduction in our fit of the energy of the triplet levels with $62 \leqslant n \leqslant 80$ and to the increase in the accuracy of our measurements.

The fitted energies are also presented in Table V. We once again extract a value for the first ionization limit: 50443.07040 cm^{-1} or 1512.2452064 THz which is compatible with the one found for the $6sns\ ^1S_0$ series with only 600 kHz difference, well below our uncertainty. This confirms our measurement stability and the completeness of the models of both series. The obtained MQDT parameters are presented in Table VIII and results are presented in Fig. 5 using a Lu-Fano representation.

VI. RITZ ENERGIES FOR HIGHER MEMBERS OF THE SERIES

While MQDT provides an excellent way to express the energies of all the members of a perturbed series, it is not particularly easy to apply. When only the energies of high-lying members of a series are required, often a simple Ritz expression is adequate. For this reason we have fitted the observed energies to a Ritz formula. The energy of the n, ℓ, j state is related to the quantum defect $\delta_{n\ell j}$ in Eq. (1). Within a specific $n\ell j$ Rydberg series, the quantum defect varies slowly with the energy and is usually described with the Ritz formula defining the quantum defect $\delta_{0,\ell j}$ at the ionization limit and additional higher-order terms $\delta_{i,\ell j}$ accounting for its energy dependence in a Taylor series. For ease of use, it is expressed as a function of the principal quantum number and thus reads

$$\delta_{n\ell j} = \delta_{0,\ell j} + \frac{\delta_{1,\ell j}}{(n-\delta_{0,\ell j})^2} + \frac{\delta_{2,\ell j}}{(n-\delta_{0,\ell j})^4} + \cdots . \quad (4)$$

For the $6sns\ ^1S_0$, $6snd\ ^1D_2$, and $6snd\ ^3D_2$ series the δ_i parameters for Eq. (4) are given in Table IX. As shown by the table the larger the n and energy range covered the more δ_i required. At low n the validity is limited by bound doubly excited perturbing states. At high n the validity can be limited by the presence of autoionizing states above the limit.

VII. DISCUSSION

The precise knowledge of the ytterbium spectra is motivated by its use as a Rydberg interacting gas and as the ion in a clock. Using high-resolution laser spectroscopy, we have measured the term energies of the $6sns\ ^1S_0$ and $6snd\ ^{1,3}D_2$ Rydberg series over $23 \leqslant n \leqslant 80$. The absolute accuracy is expected to be 7.5 MHz at one standard deviation and the observed statistical uncertainties are 2.5 MHz. We note that they are significantly lower than the expected total of 5 MHz. Each measurement corresponds to a fit of the laser excitation line over several experiments and the wavemeter's statistical measurement noise is averaged down. Complementary microwave transitions have been measured for the $6sns\ ^1S_0$–$6s(n+1)s\ ^1S_0$ intervals from $n = 34$, the $6snd\ ^1D_2$–$6s(n+1)d\ ^1D_2$ intervals from $n = 32$, and the $6s(n+1)s\ ^1S_0$–$6snd\ ^1D_2$ intervals from $n = 28$, each set complementing previous measurements. We observe typical statistical uncertainties of 0.3 MHz on level differential energies and can thus refine the optical measurements.

The combined results are fitted to an MQDT model, which characterizes these perturbed series with only a few parameters. These analyses provide an average ionization limit $I_{6s} =$ 50443.07041(25) cm^{-1}, compatible with the previously accepted value and an improved accuracy of more than 2 orders of magnitude. The inferred quantum defects correspond to a relative energy uncertainty smaller than 2.5 MHz in general, and probably smaller than 1 MHz in the microwave data range.

Although MQDT analysis of molecular spectra [48] or rare-gas Rydberg series [43] sometimes uses perturbing channels with only autoionizing levels, it is not common for other Rydberg atoms and here it is used for ytterbium. In the future, it will be possible to complete the laser spectroscopy with a three-photon excitation through $6s\,6p\ ^3P_1$ and $6s\,6d\ ^{1,3}D_2$ to $6snp$ and $6snf$ singlet or triplet levels. The precise results obtained on $6snd$ will also allow performing two-photon microwave spectroscopy towards $6sng$ levels and from these to further high-ℓ levels in the prospect of a precise calculation of the ionic core polarizability.

ACKNOWLEDGMENTS

We are grateful to F. Merkt for discussions on MQDT. T.F.G. acknowledges support from ENS Cachan and P.C.

acknowledges support from the University of Virginia for mutual visits. This work was supported by ANR program COCORYM (ANR-12-BS04-0013), the public grant CYRAQS from Labex PALM (ANR-10-LABX-0039) (P.C.), the EU H2020 FET Proactive project RySQ (Grant No. 640378), and the US Department of Energy, Office of Science, Office of Basic Energy Sciences, Chemical Sciences, Geosciences, and Biosciences Division, under Award No. DE-FG02-97ER14786.

[1] V. D. Ovsiannikov, A. Derevianko, and K. Gibble, Phys. Rev. Lett. **107**, 093003 (2011).
[2] W. Bowden, R. Hobson, P. Huillery, P. Gill, M. P. A. Jones, and I. R. Hill, Phys. Rev. A **96**, 023419 (2017).
[3] M. S. Safronova, S. G. Porsev, M. G. Kozlov, and C. W. Clark, Phys. Rev. A **85**, 052506 (2012).
[4] N. Huntemann, C. Sanner, B. Lipphardt, Chr. Tamm, and E. Peik, Phys. Rev. Lett. **116**, 063001 (2016).
[5] D. Jiang, B. Arora, M. S. Safronova, and C. W. Clark, J. Phys. B: At. Mol. Phys. **42**, 154020 (2009).
[6] R. F. Ward, Jr., W. G. Sturrus, and S. R. Lundeen, Phys. Rev. A **53**, 113 (1996).
[7] H. Weimer, M. Müller, I. Lesanovsky, P. Zoller, and H. P. Büchler, Nat. Phys. **6**, 382 (2010).
[8] M. Saffman, T. G. Walker, and K. Mølmer, Rev. Mod. Phys. **82**, 2313 (2010).
[9] M. D. Lukin, M. Fleischhauer, R. Cote, L. M. Duan, D. Jaksch, J. I. Cirac, and P. Zoller, Phys. Rev. Lett. **87**, 037901 (2001).
[10] E. Urban, T. A. Johnson, T. Henage *et al.*, Nat. Phys. **5**, 110 (2009).
[11] A. Gaëtan, Y. Miroshnychenko, T. Wilk *et al.*, Nat. Phys. **5**, 115 (2009).
[12] Y. O. Dudin and A. Kuzmich, Science **336**, 887 (2012).
[13] A. S. Bell, P. Gill, H. A. Klein, A. P. Levick, Chr. Tamm, and D. Schnier, Phys. Rev. A **44**, R20(R) (1991).
[14] W. E. Cooke, T. F. Gallagher, S. A. Edelstein, and R. M. Hill, Phys. Rev. Lett. **40**, 178 (1978).
[15] J. Millen, G. Lochead, and M. P. A. Jones, Phys. Rev. Lett. **105**, 213004 (2010).
[16] P. McQuillen, X. Zhang, T. Strickler, F. B. Dunning, and T. C. Killian, Phys. Rev. A **87**, 013407 (2013).
[17] G. Lochead, D. Boddy, D. P. Sadler, C. S. Adams, and M. P. A. Jones, Phys. Rev. A **87**, 053409 (2013).
[18] P. Schauß, M. Cheneau, M. Endres *et al.*, Nature (London) **491**, 87 (2012).
[19] G. Günter, M. Robert-de-Saint-Vincent, H. Schempp, C. S. Hofmann, S. Whitlock, and M. Weidemüller, Phys. Rev. Lett. **108**, 013002 (2012).
[20] S. K. Dutta, J. R. Guest, D. Feldbaum, A. Walz-Flannigan, and G. Raithel, Phys. Rev. Lett. **85**, 5551 (2000).
[21] S. E. Anderson, K. C. Younge, and G. Raithel, Phys. Rev. Lett. **107**, 263001 (2000).
[22] M. Saffman and T. G. Walker, Phys. Rev. A **72**, 022347 (2005).
[23] M. Aymar, A. Débarre, and O. Robaux, J. Phys. B: At. Mol. Phys. **13**, 1089 (1980).
[24] J.-F. Wyart and P. Camus, Phys. Scr. **20**, 43 (1979).
[25] P. Camus, A. Débarre, and C. Morillon, J. Phys. B: At. Mol. Phys. **13**, 1073 (1980).
[26] C. B. Xu, X. Y. Xu, W. Huang, M. Xue, and D. Y. Chen, J. Phys. B: At. Mol. Phys. **27**, 3905 (1994).
[27] M. Aymar, R. J. Champeau, C. Delsart, and O. Robaux, J. Phys. B: At. Mol. Phys. **17**, 3645 (1984).
[28] H. Maeda, Y. Matsuo, M. Takami, and A. Suzuki, Phys. Rev. A **45**, 1732 (1992).
[29] A. Osterwalder and F. Merkt, Phys. Rev. Lett. **82**, 1831 (1999).
[30] E. S. Shuman, J. Nunkaew, and T. F. Gallagher, Phys. Rev. A **75**, 044501 (2007).
[31] T. Kuwamoto, K. Honda, Y. Takahashi, and T. Yabuzaki, Phys. Rev. A **60**, 745(R) (1999).
[32] W. E. Cooke and T. F. Gallagher, Phys. Rev. A **19**, 2151 (1979).
[33] M. Kleinert, M. E. Gold Dahl, and S. Bergeson, Phys. Rev. A **94**, 052511 (2016).
[34] M. J. Seaton, Proc. Phys. Soc. London **88**, 801 (1966).
[35] M. J. Seaton, Rep. Prog. Phys. **46**, 167 (1983).
[36] J. W. Cooper, Phys. Rev. **128**, 681 (1962).
[37] U. Fano, Phys. Rev. A **2**, 353 (1970).
[38] U. Fano, J. Opt. Soc. Am. **65**, 979 (1975).
[39] M. Aymar, C. H. Greene, and E. Luc-Koenig, Rev. Mod. Phys. **68**, 1015 (1996).
[40] C. L. Vaillant, M. P. A. Jones, and R. M. Potvliege, J. Phys. B: At. Mol. Phys. **47**, 155001 (2014).
[41] A. Zuliani, Ph.D. thesis, Université Paris-Saclay, 2015.
[42] K. T. Lu and U. Fano, Phys. Rev. A **2**, 81 (1970).
[43] C.-M. Lee and K. T. Lu, Phys. Rev. A **8**, 1241 (1973).
[44] J. A. Armstrong, P. Esherick, and J. J. Wynne, Phys. Rev. A **15**, 180 (1977).
[45] O. Robaux and M. Aymar, Comput. Phys. Commun. **25**, 223 (1982).
[46] W. E. Cooke and C. L. Cromer, Phys. Rev. A **32**, 2725 (1985).
[47] J. M. Lecomte, J. Phys. B: At. Mol. Phys. **20**, 3645 (1987).
[48] A. Osterwalder, A. Wüest, F. Merkt, and C. Jungen, J. Chem. Phys. **121**, 11810 (2004).